Adv. Geosci., 42, 73–81, 2016
www.adv-geosci.net/42/73/2016/
doi:10.5194/adgeo-42-73-2016

Advances in Geosciences
Open Access
EGU

Tropical and Extratropical predictions of the summer and autumn Niño3.4 Index: a comparison

Miguel Tasambay-Salazar[1,2], María José OrtizBeviá[1], Antonio RuizdeElvira[1], and Francisco José Alvarez-García[1]

[1]Departamento de Física y Matemática, Universidad de Alcalá, Alcalá de Henares, 28801, Spain
[2]Facultad de Informática y Electrónica, Escuela Superior Politécnica de Chimborazo, Riobamba, EC060155, Ecuador

Correspondence to: Miguel Tasambay-Salazar (mtasambay@espoch.edu.ec)

Received: 31 March 2016 – Revised: 5 August 2016 – Accepted: 13 August 2016 – Published: 26 August 2016

Abstract. The El Niño-Southern Oscillation (ENSO) phenomenon is the main source of the predictability skill in many regions of the world for seasonal and interannual timescales. Longer lead predictability experiments of Niño3.4 Index using simple statistical linear models have shown an important skill loss at longer lead times when the targeted season is summer or autumn. We develop different versions of the model substituting some its variables with others that contain tropical or extratropical information, produce a number of hindcasts with these models using two different predictions schemes and cross validate them. We have identified different sets of tropical or extratropical predictors, which can provide useful values of potential skill. We try to find out the sources of the predictability by comparing the sea surface temperature (SST) and heat content (HC) anomalous fields produced by the successful predictors for the 1980–2012 period. We observe that where tropical predictors are used the prediction reproduces only the equatorial characteristics of the warming (cooling). However, where extratropical predictors are included, the predictions are able to simulate the absorbed warming in the South Pacific Convergence Zone (SPCZ).

1 Introduction

The El Niño-Southern Oscillation (ENSO) is the dominant interannual climatic signal and the main source of the predictability skill in many regions of the world for seasonal and interannual timescales. Improving the ENSO understanding and forecast skill is still one of the main goals of international seasonal forecast programs (Kirtman et al., 2013). The ENSO impacts in many regions of the world opens an opportunity window for forecast in those regions. The monthly Climate Diagnostics Bulletin (CDB; http://www.cpc.ncep.noaa.gov/products/CDB/CDB_Archive_html/CDB_archive.shtml) publishes a variety of ENSO forecasts. A feature found in the analysis of all CDB forecasts is the skill loss at a lead time of three or more seasons ("the longer lead forecasts").

The phenomenon El Niño depends on factors that include interactions between the tropics and extratropics that affect its behavior (Philander, 1999). In a previous work (Tasambay-Salazar et al., 2015a) we have determined the feedbacks between ENSO and teleconnection indexes from other regions of the world. In the present work, the Niño3.4 Index characterizes the ENSO variability and the variability of the other regions is represented by some other indexes. Some of these, as the Southern Oscillation Index, or the Pacific Western Equatorial Heat Content Index, representing the equatorial or the tropical Pacific state, have been used in many studies for ENSO forecasts studies (Barnston and Livezey, 1987; Penland and Magorian, 1993; Zebiak and Cane, 1987). Other, that represent the variability outside of the tropical Pacific basin, were suggested or used as predictors in the most recent literature. Among the ENSO precursors external to the tropical Pacific disclosed by recent studies we count some signals in the tropical Indian ocean (Izumo et al., 2010; Luo et al., 2010) or the tropical Atlantic (Keenlyside et al., 2013; Rodríguez-Fonseca et al., 2009). Other novel research like Stepanov (2009); Terray (2011); Vimont et al. (2009) or Ballester et al. (2011) point to the potential of some extratropical variability the North Pacific, the Antartic current at its Indian, Atlantic or Pacific sectors, for ENSO predictability.

In two recent papers, Tasambay-Salazar et al. (2015a, b) have introduced some of these novel precursors in a series of simple seasonal stochastic model in order to study the characteristics of the predictability of the equatorial Pacific, represented by the Niño3.4, the Niño4 and the Niño1 + 2 indexes. The model parameters were identified from data of the recent post-satellite period (1980–2012). In these studies, we used as benchmarks a basic equatorial model, which variables represent the part played by the surface ocean, the subsurface ocean and the atmosphere in the ENSO phenomenon. These three variables are the corresponding Niño Index, an index for the anomalous heat content in the equatorial Pacific, and the Southern Oscillation Index. It was found that the differences among the model's skills were more evident when the hindcasts were performed across the spring. Then the model faced the "spring predictability barrier". In these conditions, only the model versions that include a representation of the extratropical feedbacks among its variables were able to provide useful hindcast skills.

The models employed in Tasambay-Salazar et al. (2015a, b) were built on the basis of some feedback relationships, identified from the lead-lag correlation coefficient values between the corresponding Niño Index and each of the other indexes. In Tasambay-Salazar et al. (2015a) we compared the feedbacks relationship identified in the previous (1950–1979) with those obtained for the post satellite period. In the case of the Niño3.4 Index, the only variable identified with a predictive potential for both periods was the equatorial Pacific anomalous heat content. The performance of the models was assessed by two parameters, correlation skill and root mean square error.

In the present work, however, we present some other measures of the adequacy of the models, like its performance at hindcasting extreme and normal conditions, or at simulating some basic physical variables, like the sea surface temperature anomalies or the heat content anomalies in the tropical Pacific. Details on the datasets used, the procedures followed for the variables identification and the models are given in Sect. 2. The results of the analysis are presented in Sect. 3, and we finish with some concluding remarks in Sect. 4.

2 Data and Methods

The ENSO state that represents the Niño3.4 Index is obtained as an average of the monthly SST anomalies in the region (5° N–5° S, 120–170° W). Other variables used in the first part of this work (for the Tropical or T-model) are the Southern Oscillation Index (SOI), defined as the difference between the standardized anomalies of Sea Level Pressure of Darwin and Tahiti (Trenberth, 1997), and the WWV Index, obtained by averaging the equatorial warm water volume (WWV) anomalies across the Pacific basin computed by the Australian Bureau of Meteorology Research (Meinen and McPhaden, 2000). Another variable included for the longer lead experiment is the Middle Tropospheric Temperature (MTT) Index. This last index was produced by averaging the observed atmospheric temperature variability integrated from the surface up to the middle troposphere of the tropical band. All of these indexes were taken from the US National Oceanic and Atmospheric Administration (NOOA). Due to the limitations in the availability of satellite data, our analysis only covers the time interval from 1980 to 2012. According to Trenberth (1997) criterion, anomalous positive (negative) ENSO events were identified from the Niño3.4 Index (ONI) when this last's value was above (or below) the value of 0.4 °C for 6 or more months. In this study, we have identified 9 warm and 9 cold events that took place according to with the above criterion during the chosen period. The seasonal values are defined as three months averages, starting with winter values obtained from the December, January, and February (DJF) monthly values and so on.

In addition to the Niño3.4 Index, the models that incorporate extratropical predictors use indexes obtained from an analysis of covariance of the seasonal anomalies of some global oceanic and regional atmospheric fields. The basic oceanic field is the global SST field from ERA-Interim reanalysis (Dee et al., 2011) at a spatial grid of $0.5° \times 0.5°$. Typically for winter and summer, the first Principal Component (PC) of this field carries most of the field trend, explaining 36 % of the variance, while the PCs of order higher than the tenth explain less than 3 % of the variance. Occasionally, we use another global oceanic field, the deep 300 m Heat Content field (HC300) at a grid of $1° \times 1°$, which is obtained from the Simple Ocean Data Analysis (SODA) (Carton and Giese, 2008). In the case of atmospheric variables, we use the recently released global MTT field (Mears and Wentz, 2009) at a grid of $2.5° \times 2.5°$. The variables were identified from the Principal Components (PCs) of the MTT anomalies in the North Pacific (NP) from (20–90° N, 120° E–120° W) or from the PCs of the Global Southern Extratropic (GSE) domain (20–90° S). Although there is an evident trend in the MTT fields for a given season, the trend is mostly confined to the 1st PC of the field (explaining 26 % of the variability). In the results presented here, no trend removal was applied because the variables selected do not show a significative trend. The selection of the variables was based on the significance of the PC correlation coefficient with the Niño3.4 Index at a lag time equal to the forecast lead. In some complementary experiments, we use the PCs from sectors of the GSE, as detailed in Table 1.

Let all variables of the model $\boldsymbol{y}_i(t)$ (including the one that represents the ENSO state) be collected in a seasonal state vector $\boldsymbol{y}$. Following Hasselmann (1988), we model their evolution in time by the following set of equations:

$$\frac{\mathrm{d}\boldsymbol{y}}{\mathrm{d}t} = \mathbf{A}\boldsymbol{y} + \boldsymbol{n} \tag{1}$$

where $\mathbf{A}$ is the dynamical or feedback matrix that represents the effects that the present state of the variables has on the evolution of each variable and $\boldsymbol{n}$ represents the forcing noise

Table 1. Acronyms and specifications of the regions used to build the extratropical predictors.

Acronym	Region	Latitude	Longitude
NP	North Pacific	20–90° N	120° E–120° W
SP	Southern Pacific	20–90° S	160° E–80° W
GSE	Global South Extratropic	20–90° S	0–360°
RB	Ross-Bellingshausen	60–90° S	160° E–60° W
SPA	Southern Pacific Antarctic	50–90° S	160° E–80° W
SAIA	Southern Atlantic and Indian Antarctic	50–90° S	60° W–150° E
SAI	Southern Atlantic and Indian	20–90° S	60° W–150° E

assumed to be stationary Gaussian and delta correlated. Let us collect the $\boldsymbol{m}$ available observations of the state vector $\boldsymbol{y}$ in a $(\boldsymbol{n} \times \boldsymbol{m})$, $\mathbf{Y}$ matrix. If $\boldsymbol{m}$ is big enough, the $\mathbf{A}$ matrix can be identified from the data second moments statistics. The eigenvectors of the $\mathbf{A}$ matrix yield the new spatial basis $\mathbf{U} = \{\boldsymbol{u}_i\}$. Because the $\mathbf{A}$ matrix is generally non-symmetric, the complex eigenvalues represent an oscillatory mode. On this ground, the new basis vectors $\boldsymbol{v}$, built as

$$im\{\lambda_i\} = 0, \ \boldsymbol{v}_i = \boldsymbol{u}_i \tag{2a}$$

$$im\{\lambda_i\} \neq 0, \ \boldsymbol{v}_i = Re\{\boldsymbol{u}_i\}, \ \boldsymbol{v}_{i+1} = Im\{\boldsymbol{u}_i\} \tag{2b}$$

are usually called the Principal Oscillation Patterns (POP) of the system (Hasselmann, 1988). More details about the seasonal version of the POP analysis used here can be found in Tasambay-Salazar et al. (2015b). The temporal evolution of the $\boldsymbol{V}$ vectors, $\mathbf{T}$, is obtained by projecting the $\mathbf{Y}$ data into the $\boldsymbol{V}$ vectors

$$\mathbf{T} = \boldsymbol{V}^{-1}\mathbf{Y} \tag{3}$$

Here, we measure the potential skill (PS) of the model using a linear correlation coefficient (r) at different lags between the Niño3.4 Index at summer (autumn) season and each of the other indexes to identify a linear relationship that will indicate a potential predictability. We have used two different predictive schemes, the first one, with the POP evolution scheme (Von Storch et al., 1995), hereinafter labelled as OS, for Optimised Signal or simply "without noise" and the second one, following the approach (Penland and Matrosova, 1998) that include some characteristics of the noise into the hindcast, hereinafter FSM for Full Stochastic Model or simply "with noise". More details can be found in a recent work of Tasambay-Salazar et al. (2015b). By analogy with the synoptic forecast case, skill values are considered useful only if they exceed the 0.6 threshold value (Hollingsworth et al., 1980). Due to the limited availability in time of the satellite fields, all the available data are used for the determination of the model parameters.

In order to further assess the performance of the models, we compare the patterns of the tropical SST and HC fields simulated with the most successful models with the observed ones. These patterns were obtained by correlation the corresponding hindcasted of observed indexes onto those fields.

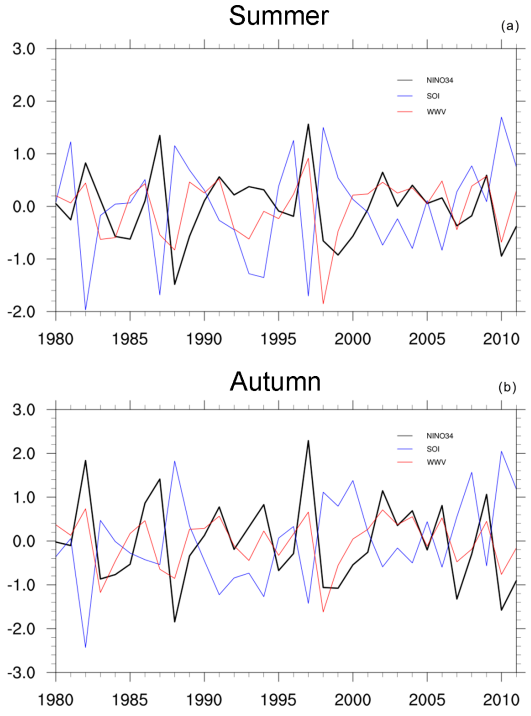

Figure 1. Niño3.4, SOI and WWV indexes in summer (Fig. 1a) and Niño3.4, SOI and WWV indexes in autumn (Fig. 1b).

Additionally, we separate the skill obtained when hindcasting El Niño (or La Niña) situations from the skill of the hindcasts issued for ENSO-neutral conditions. In this way, we are able to identify those configurations that have very good skill with the ENSO anomalous phases from those that correspond to normal situations.

3 Results and Discussion

The Tropical or T-model used here as a benchmark was chosen as the most successful of several tropical models, with different configurations. We use basically three indexes, the Niño3.4 Index and the SOI Index and the WWV Index (NSW model). These Indexes are represented in Fig. 1a for the summer model and in Fig. 1b for the autumn model. Some other

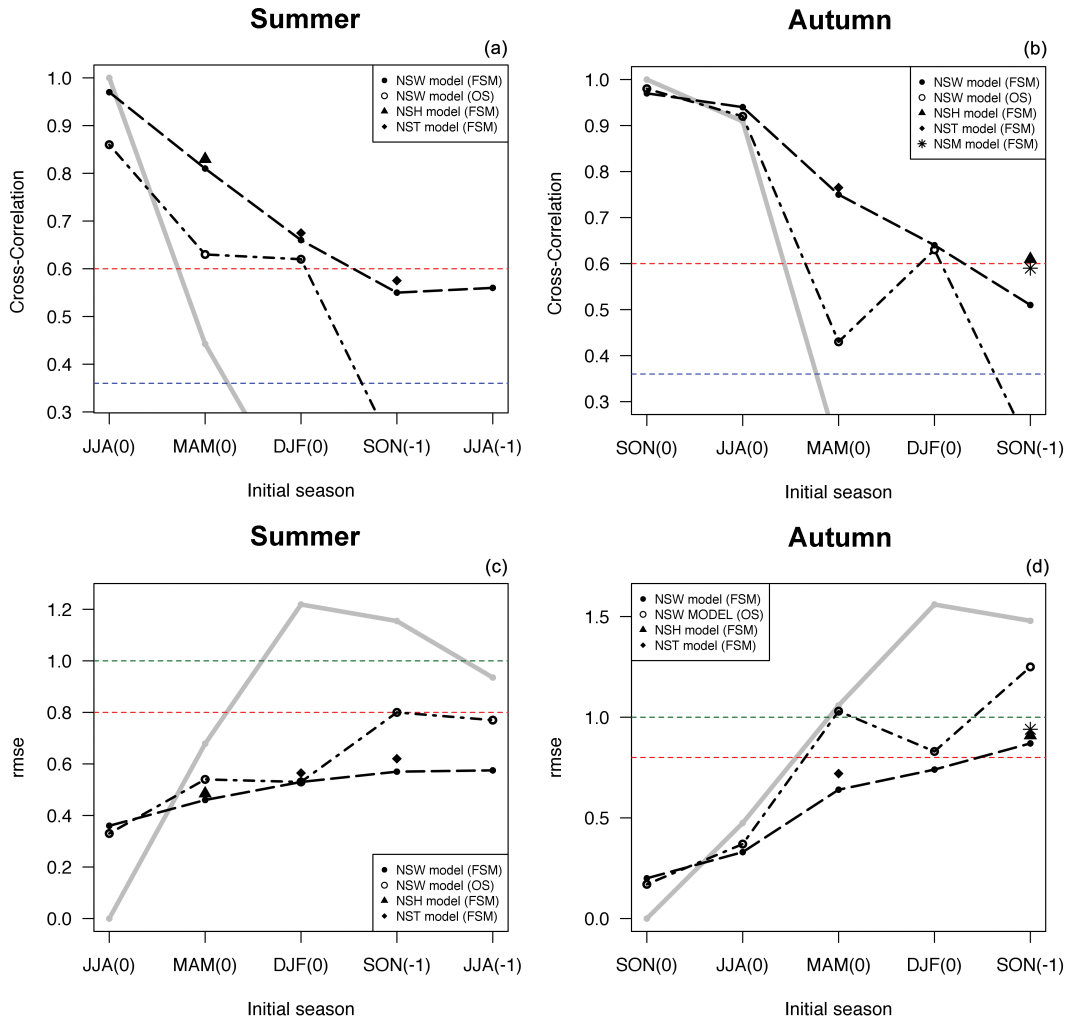

Figure 2. Seasonal cross-correlation of the Niño3.4 Index hindcast with the NSW model in **(a)** summer and **(b)** autumn. Different versions of the stochastic T-model: the NSW model under FSM scheme (filled circle), the NSW model under OS scheme (empty circle), the NSH model under FSM scheme (triangle), the NST model under FSM scheme (diamond), and the NWM model under FSM scheme (asterisk). On the background, the solid gray line represents the cross-correlation of the hindcast produced assuming the Niño3.4 Index persistence. The blue straight dashed line indicates the statistical significance threshold at 95 % confidence level. The red dashed straight line represents an arbitrary threshold for the useful forecast as proposed by Hollingsworth et al. (1980). Panels **(c)** and **(d)** shown the seasonal cross-RMSE of the Niño3.4 Index hindcasted with the NSW model and others versions of the stochastic T-model in summer and autumn, respectively. On the background, the solid gray line represents the cross-RMSE of the hindcast produced assuming the Niño3.4 Index persistence. The blue straight dashed line indicates the statistical significance threshold at 95 % confidence level. Finally, The red dashed straight line represents an arbitrary threshold for the useful forecast as derived by Hollingsworth et al. (1980).

models are built by replacing one of the two basic Indexes other than the Niño3.4 index, as for instance, the NSH model (include a index from heat content field), the NST model (include a index from sea surface temperature field), the NSM model (include a index from middle tropospheric field). The PS scores (seasonal cross-correlation coefficients) of these predictions for Niño3.4 Index at each season and for different lead times are presented in Fig. 2a (summer) and in Fig. 2b (autumn), their seasonal cross-RMSE hindcasted (calculated by RMSE of the seasonal cross-correlation hindcasted previously) are depicted in Fig. 2c and d, respectively. The deterioration of the predictability at lead times greater than two seasons in the case of summer and greater than three seasons in the case of autumn is evident there. We can observe that using the more sophisticated FSM prediction scheme produces useful PS values at leads up to two seasons for summer and at leads up to three seasons in the case of autumn. The measure of the forecast skill given by the root mean square error (RMSE) (represented in Fig. 2c and d) is better for FSM prediction scheme, assuming the persistence of the Niño3.4 values, which are represented by a continuous gray line. The inclusion of extra equatorial information (either surface or

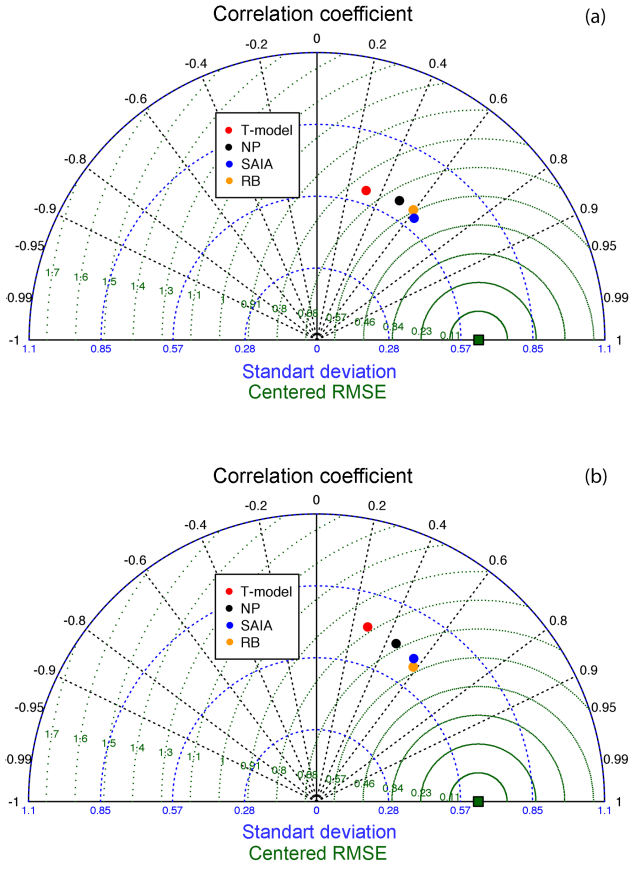

Figure 3. **(a)** Statistical comparison between cross-correlation, cross-RMSE correlation and standard deviation (Taylor diagram) of the hindcasts for the summer SST field performed with different models initialized in summer. The model variables are the Niño3.4 Index, the WWV Index and another index identified from different extratropical regions: NP (black), SAIA (purple) and RB (orange). T-model is depicted with a red circle. **(b)** as in **(a)** but for the summer HC field.

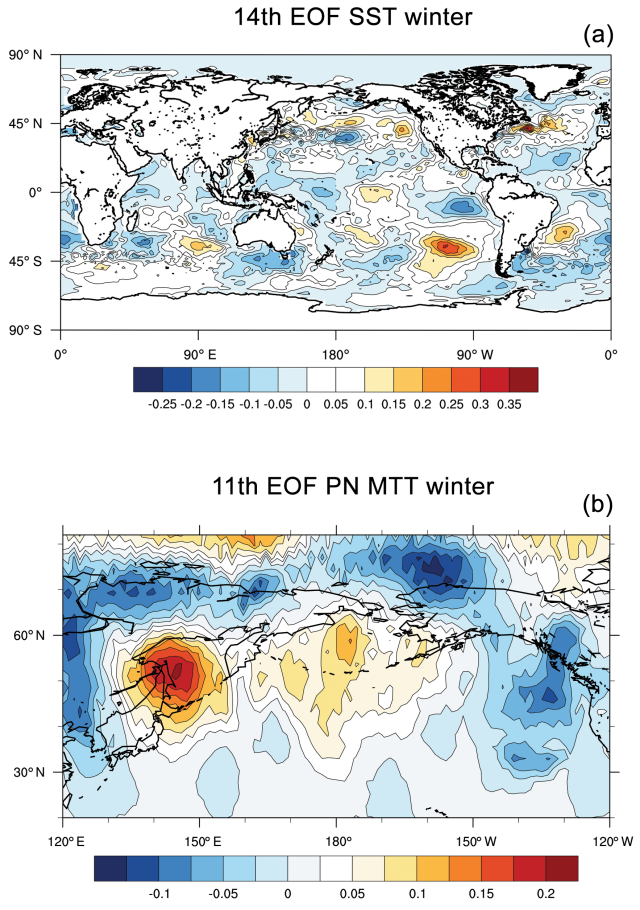

Figure 4. **(a)** The spatial pattern (EOF) associated with the 14th PC of the SST winter field used for the prediction Niño3.4 Index. **(b)** the spatial pattern (EOF) associated with the 11th PC of MTT winter field that was also used for those predictions.

subsurface) somewhat improves the PS values for the predictions of the summer Niño3.4 Index at longer lead times. We omit the results in the case of the winter and spring predictions, whereas previously mentioned the PS values remain above 0.7 at lead times up to one year.

Some of the models that use extratropical predictors are able to somehow improve the PS values. Their performance is summarized and depicted for the SST and HC summer fields in the Taylor diagrams depicted in Fig. 3a and b, respectively. We can appreciate that the skill correlation coefficients of the models whose variables were obtained from SAIA or RB regions are above the useful threshold. The relevant traits of the patterns of those PCs included in the configurations that scored higher PS values are represented in the Figs. 4 and 5. In the case of the Niño3.4 Index summer predictions, the 14th PC of the SST global field and the 11th PC of the MTT North Pacific field seem to be the only winter variables that are able to produce useful PS values. The corresponding Empirical Orthogonal Functions (EOF) are represented in Fig. 4a and b. In the oceanic pattern, there are cooling anomalies in the Eastern and Central NP and warming anomalies above. There is also a dipole in the Eastern Pacific, with an incipient cooling in the Niño3 region. In the atmospheric MTT pattern, the horseshoe-cooling pattern over land is similar to the upper wind field associated with the seasonal footprinting by Anderson (2004). Some traits of the oceanic pattern combined with the reduced amount of variance explained support the view that these variables should be included in the T-models as noise, as suggested by Penland and Sardeshmukh (1995).

The summer predictors that score the highest PS values are the 15th PC of the global SST field and the 3rd and 5th PCs of the GSE MTT field. In the case of the summer MTT variables, the 3rd, and 5th PCs explain 12 and 7 %, respectively, of the total variance. The SST 15th PC and the GSE MTT 3rd PC are also included in most of the configurations found useful for the autumn prediction. The corresponding SST

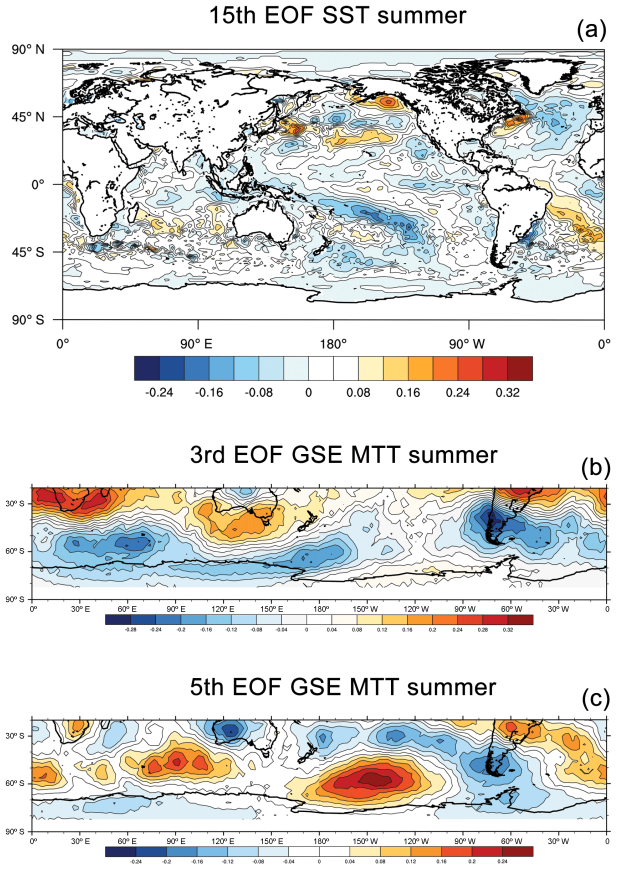

Figure 5. **(a)** The spatial pattern (EOF) associated with the 15th PC of the SST field used for the prediction of the summer Niño3.4 Index. **(b)** and **(c)** represent the spatial pattern (EOF) associated with the 3rd PC and the 5th PC, respectively, of the GSE MTT field that was also used for those predictions. Notice the propagation of features between **(b)** and **(c)**.

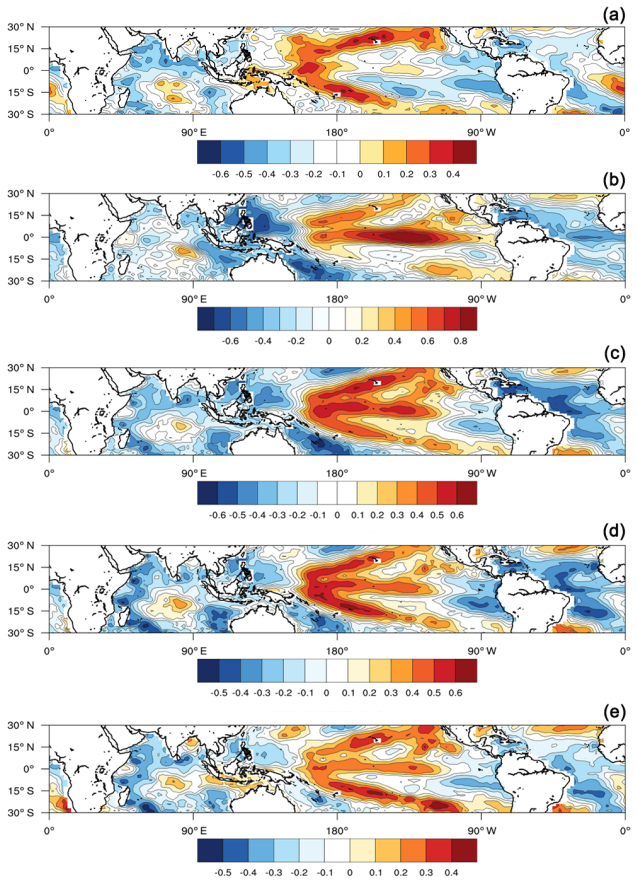

Figure 6. **(a)** The summer SST field reconstructed from the observations, from **(b–e)** represent the correlations maps between the summer SST field and the time coefficients of the T-model, NP, SAIA and RB region, respectively.

EOF, in Fig. 5a shows an anomalous cooling in the South Pacific Convergence Zone. In Fig. 5b, the 3rd GSE MTT EOF displays wavelike activity in the Antarctic Circumpolar Current (ACC) region, with three maxima located near the Shackelton Ridge, the Ross region and over the Patagonia sector and topped by anomalies of opposite sign at the lower latitudes. In the 5th GSE MTT EOF, depicted in Fig. 5c, the maxima, which have opposite signs, are displaced approximately 40° to the east. Similar features were detected in the ACCs by previous studies related to ENSO impacts in the region (Holland et al., 2005; Verdy et al., 2006). The westerly wind anomalies induced by ENSO would produce anomalous sea ice export, the appearance of ice-free ocean areas and anomalies in the upper level convergence field. Rossby waves would propagate the induced atmospheric anomalies to the mid-latitudes, consequently inducing warm and cold anomalies in key tropical regions.

The snapshots in the Figs. 6 and 7 represent the forecasted SST (Fig. 6) and HC (Fig. 7) fields. They were constructed by regressing the forecasted time coefficient into the respective fields. The Figs. 6a and 7a represent the SST and HC fields reconstructed from the observations, respectively. We can appreciate in Fig. 6a the characteristic SST anomaly in the Western Pacific, traveling to the east that signals the first stages of an El Niño event. The HC pattern represented in Fig. 7a corresponds also to an El Niño initial stage. The Figs. 6b and 7b presents the SST and HC fields reconstructed with equatorial predictors, and correspond to an already developed El Niño warming. Notice how in the warm anomalies in the HC field are confined to the equatorial region. The patterns in the Figs. 6c and 7c were obtained using NP predictors, and show a clear El Niño warm episode, that is, however less developed that the one obtained with the equatorial model. In the case of the Figs. 6d and 7d, the patterns were obtained using predictors from the South Atlantic and Indian Antarctic sectors and more similar to the ones obtained with the observation than the preceding ones. The Figs. 6e and 7e were produced with predictors obtained through a statistical analysis of the Ross-Bellingshausen region (RB). The phase

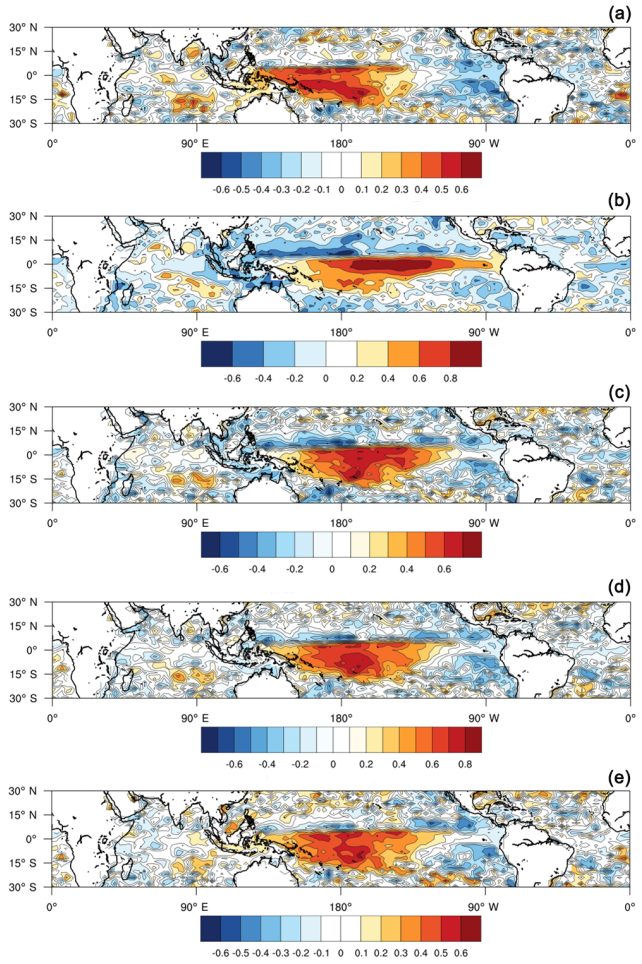

Figure 7. (a) The summer HC field reconstructed from the observations, from **(b–e)** represent the correlations maps between the summer HC field and the coefficients temporary of T-model, NP, SAIA and RB region, respectively.

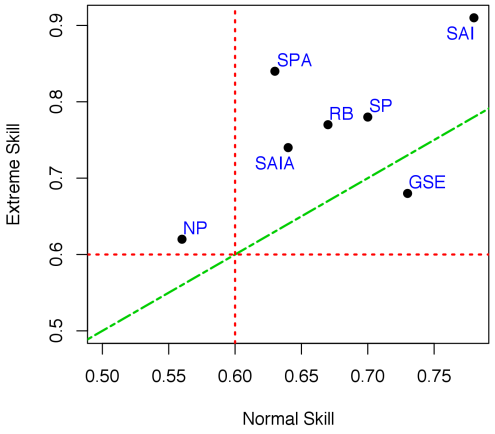

Figure 8. Performance models for normal and extreme conditions. The horizontal axis corresponds to normal skill and the vertical axis to the extreme skill. The green straight dashed line indicates the reference for equal values of the hindcast skill corresponding to anomalous ENSO conditions and those for the ENSO-neutral state. The red dashed straight lines represent an arbitrary threshold for the useful forecast as proposed by Hollingsworth et al. (1980). The acronyms correspond to a model configuration in the different regions, as detailed in Table 1.

of the El Niño warming represented by the last patterns corresponds well to the one obtained with the observations. Furthermore, we have separated the skill values of the hindcast that target anomalous ENSO conditions from the ones issued for ENSO-neutral states.

In Fig. 8, we can observe the performance models for normal and extreme conditions. The horizontal axis corresponds to normal skill and the vertical axis to the extreme skill. The green straight dashed line indicates the reference for equal values of the hindcast skill corresponding to anomalous ENSO conditions and those for the ENSO-neutral state. The red dashed straight lines represent an arbitrary threshold for the useful forecast as proposed by Hollingsworth et al. (1980), the acronyms correspond to a model configuration as detailed in Table 1. We can observe that the best hindcast skill value for the extreme and the normal conditions correspond to predictors from SAI region. A possible explanation of this behaviour could be due to the water mass formation that occurs in this region provides important links to the global ocean circulation, allowing variability in the Southern Ocean to affect global climate conditions. Additionally, the ACC system acts as the only direct link connecting the world's major ocean basins, allowing for signals to be transmitted directly among these basins according to Holland et al. (2005) or Verdy et al. (2006). Another hand, the hindcast skill prediction obtained from GSE region achieves similar values for extreme and normal conditions. This applies also to models that use predictors obtained from the NP region, but with no useful skill for normal conditions.

We have identified that best value hindcast skill of extreme conditions was obtained by the model uses the 7th PC in the SAI sector of the MTT field, while the best value hindcast skill of normal conditions is provided by a model that uses the 3rd PC in the SAI sector of the MTT field. In the configurations that use predictors from the SPA and NP sectors, the model uses the 2nd and the 1st PCs of the MTT field. It is important to highlight that all the retained configurations included among their variables the 15th PC of the SST field.

4 Conclusions

In this work, we investigate the factors that determine the longer lead ENSO predictability. ENSO state is represented by the seasonal value of the Niño3.4 Index. ENSO predictability is measured by the hindcast skill of a number of simple empirical models. The variables used for the model's configuration were identified by a feedback analysis in a previous study. The skill of the hindcasts obtained by models

built from equatorial and tropical Pacific variables serve as benchmarks against which all the others are compared.

In the previous study, we found that the low PS values that characterize the ENSO longer lead predictions are mainly a consequence of the low PS values of the predictions that target the summer and autumn Niño3.4 conditions when using only tropical predictors. To improve these PS values, we build a number of models that include the extratropical processes and regions identified as longer lead ENSO precursors by previous studies. Among these precursors are the NP region, the ACC region, the RB dipole or the Southern Atlantic and Indian Oceans. Although some of these precursors were used for predictions in a previous work (Dominiak and Terray, 2005), no study has provided a detailed comparison of their predictive capabilities. A second novelty of the present work is the inclusion of variables derived from the MTT field in the model.

The results obtained there with the T-model indicate that introducing the variability of the tropical ocean or atmosphere into the model yields better the PS values at longer leads for the summer and autumn Niño3.4. Index. They also show that further improvements of the longer lead PS can be achieved by introducing extratropical information in the model variables. The analysis of many sensitivity experiments revealed that the higher PS scores correspond to configurations that include variables representing global SST and regional MTT anomalies. The results also present a dependence on the seasonal signature of the initial conditions, which is in agreement with the "seasonal footprinting" concept.

The results of previous works also shown that there were ensembles of configurations yielding similar values of PS. The present study investigates other measures than the PS that can help us to select one or other configuration as the most appropriate. One of these is the quality of the reconstruction of the key SST and HC tropical anomalies obtained with those models. Among the configuration analyzed the ones that include MTT variables obtained from the RB or from the SAIA sectors are the ones that provide a better representation of those fields conditions in the Tropical Pacific compared with the observed ones. We notice that when using tropical predictors the prediction reproduces only the equatorial characteristics of the warming (cooling) events while when considering extratropical predictors the predictions are able to simulate the warming in the South Pacific Convergence Zone (SPCZ) that appear in the observations.

The other approach followed here consists in separating the PS values obtained for hindcasts of anomalous (positive or negative) ENSO conditions from those where ENSO is in a neutral state. In this context, we found models that achieve very good performances when targeting the anomalous ENSO conditions and rather loosely ones when hindcasting neutral conditions, and other do the opposite. Moreover, there are other models that have a similarly good performance in both situations. To the first class belong models that include variables that are ahead of the predictand when the maximum value of the correlation coefficient is reached, like the 7th PC of the MTT. To the second class belong those models that have good skill at hindcasting normal conditions although the reasons remain yet unexplained. In the third category (the all-terrain) are the models that include variables that have important correlation for both, negative and positive lags with respect summer Niño3.4 Index.

5 Data availability

The ERA-Interim SST data used in this paper are available from the European Centre for Medium-Range Weather Forecasts (http://www.ecmwf.int/en/research/climate-reanalysis/era-interim). Climate Indexes, the MTT field and the SODA data were obtained from NOAA (http://www.cpc.noaa.gov).

Acknowledgements. We thank the supporting of SENESCYT – Ecuador. Some of the figures were produced using the NCAR Command Language (NCL) software package (version 6.1.2.).

Edited by: J. D. Pabón-Caicedo
Reviewed by: J. J. Velez and one anonymous referee

References

Anderson, B.: Investigation of a Large-Scale Mode of Ocean – Atmosphere Variability and Its Relation to Tropical Pacific Sea Surface Temperature Anomalies, 17, 4089–4098, 2004.

Ballester, J., Rodríguez-Arias, M., and Rodó, X.: A new extratropical tracer describing the role of the western Pacific in the onset of El Niño: Implications for ENSO understanding and forecasting, J. Climate, 24, 1425–1437, doi:10.1175/2010JCLI3619.1, 2011.

Barnston, A. G. and Livezey, R. E.: Classification, Seasonality and Persistence of Low-Frequency Atmospheric Circulation Patterns, Mon. Weather Rev., 115, 1083–1126, http://dx.doi.org/10.1175/1520-0493(1987)115<1083:CSAPOL>2.0.CO;2, 1987.

Carton, J. A. and Giese, B. S.: A Reanalysis of Ocean Climate Using Simple Ocean Data Assimilation (SODA), Mon. Weather Rev., 136, 2999–3017, doi:10.1175/2007MWR1978.1, 2008.

Dee, D. P., Uppala, S. M., Simmons, A. J., Berrisford, P., Poli, P., Kobayashi, S., Andrae, U., Balmaseda, M. A., Balsamo, G., Bauer, P., Bechtold, P., Beljaars, A. C. M., van de Berg, L., Bidlot, J., Bormann, N., Delsol, C., Dragani, R., Fuentes, M., Geer, A. J., Haimberger, L., Healy, S. B., Hersbach, H., Hólm, E. V., Isaksen, L., Kallberg, P., Kohler, M., Matricardi, M., Mcnally, A. P., Monge-Sanz, B. M., Morcrette, J. J., Park, B. K., Peubey, C., de Rosnay, P., Tavolato, C., Thépaut, J. N., and Vitart, F.: The ERA-Interim reanalysis: Configuration and performance of the data assimilation system, Q. J. Roy. Meteor. Soc., 137, 553–597, doi:10.1002/qj.828, 2011.

Dominiak, S. and Terray, P.: Improvement of ENSO prediction using a linear regression model with a southern Indian Ocean sea surface temperature predictor, Geophys. Res. Lett., 32, 1–4, doi:10.1029/2005GL023153, 2005.

ECMWF: ERA-Interim SST data, available at: http://www.ecmwf.int/en/research/climate-reanalysis/era-interim, last access: 18 August 2016.

Hasselmann, K.: PIPs and POPs: The reduction of complex dynamical systems using principal interaction and oscillation patterns, J. Geophys. Res., 93, 11015, doi:10.1029/JD093iD09p11015, 1988.

Holland, M. M., Bitz, C. M., and Hunke, E. C.: Mechanisms forcing an Antarctic dipole in simulated sea ice and surface ocean conditions, J. Climate, 18, 2052–2066, doi:10.1175/JCLI3396.1, 2005.

Hollingsworth, A., Arpe, K., Tiedtke, M., Capaldo, M., and Savijärvi, H.: The Performance of a Medium-Range Forecast Model in Winter – Impact of Physical Parameterizations, Mon. Weather Rev., 108, 1736–1773, doi:10.1175/1520-0493(1980)108<1736:TPOAMR>2.0.CO;2, 1980.

Izumo, T., Vialard, J., Lengaigne, M., de Boyer Montegut, C., Behera, S. K., Luo, J.-J., Cravatte, S., Masson, S., and Yamagata, T.: Influence of the state of the Indian Ocean Dipole on the following year's El Niño, Nat. Geosci., 3, 168–172, doi:10.1038/ngeo760, 2010.

Keenlyside, N. S., Ding, H., and Latif, M.: Potential of equatorial Atlantic variability to enhance El Niño prediction, Geophys. Res. Lett., 40, 2278–2283, doi:10.1002/grl.50362, 2013.

Kirtman, B., Anderson, D., Brunet, G., Kang, I., Scaife, A., and Smith, D.: Prediction from weeks to decades, in: Climate science for serving, 205–235, doi:10.1007/978-94-007-6692-1, 2013,

Luo, J. J., Zhang, R., Behera, S. K., Masumoto, Y., Jin, F. F., Lukas, R., and Yamagata, T.: Interaction between El Niño and extreme Indian Ocean dipole, J. Climate, 23, 726–742, doi:10.1175/2009JCLI3104.1, 2010.

Mears, C. A. and Wentz, F. J.: Construction of the remote sensing systems V3.2 atmospheric temperature records from the MSU and AMSU microwave sounders, J. Atmos. Ocean. Tech., 26, 1040–1056, doi:10.1175/2008JTECHA1176.1, 2009.

Meinen, C. S. and McPhaden, M. J.: Observations of Warm Water Volume Changes in the Equatorial Pacific and Their Relationship to El Niño and La Niña, J. Climate, 13, 3551–3559, doi:10.1175/1520-0442(2000)013<3551:OOWWVC>2.0.CO;2, 2000.

NOAA: Climate Indexes, MTT field and the SODA data, available at: http://www.cpc.noaa.gov, last access: 18 August 2016.

Penland, C. and Magorian, T.: Prediction of Niño3 sea surface temperatures using linear inverse modeling, J. Climate, 6, 1067–1076, doi:10.1175/1520-0442(1993)006<1067:PONSST>2.0.CO;2, 1993.

Penland, C. and Matrosova, L.: Prediction of Tropical Atlantic Sea Surface Temperatures Using Linear Inverse Modeling, J. Climate, 11, 483–496, doi:10.1175/1520-0442(1998)011<0483:POTASS>2.0.CO;2, 1998.

Penland, C. and Sardeshmukh, P. D.: The Optimal Growth of Tropical Sea Surface Temperature Anomalies, J. Climate, 8, 1999–2024, doi:10.1175/1520-0442(1995)008<1999:TOGOTS>2.0.CO;2, 1995.

Philander, S. G.: A review of tropical ocean-atmosphere interactions, Tellus B, 51, 71–90, doi:10.3402/tellusa.v51i1.12307, 1999.

Rodríguez-Fonseca, B., Polo, I., García-Serrano, J., Losada, T., Mohino, E., Mechoso, C. R., and Kucharski, F.: Are Atlantic Niños enhancing Pacific ENSO events in recent decades?, Geophys. Res. Lett., 36, L20705.1–L20705.6, doi:10.1029/2009GL040048, 2009.

Stepanov, V. N.: Modeling of El Niño events using a simple model, Oceanology, 49, 310–319, doi:10.1134/S0001437009030023, 2009.

Tasambay-Salazar, M., OrtizBeviá, M. J., Alvarez-García, F. J., and RuizdeElvira, A. M.: An estimation of ENSO predictability from its seasonal teleconnections, Theor. Appl. Climatol., 122, 383–399, doi:10.1007/s00704-015-1546-3, 2015a.

Tasambay-Salazar, M., OrtizBeviá, M. J., Alvarez-García, F. J., and RuizdeElvira, A. M.: The Niño3.4 region predictability beyond the persistence barrier, Tellus A, 67, 1–17, doi:10.3402/tellusa.v67.27457, 2015b.

Terray, P.: Southern Hemisphere extra-tropical forcing: A new paradigm for El Niño-Southern Oscillation, Clim. Dynam., 36, 2171–2199, doi:10.1007/s00382-010-0825-z, 2011.

Trenberth, K. E.: The Definition of El Niño, B. Am. Meteorol. Soc., 78, 2771–2777, doi:10.1175/1520-0477(1997)078<2771:TDOENO>2.0.CO;2, 1997.

Verdy, A., Marshall, J., and Czaja, A.: Sea surface temperature variability along the path of the antarctic circumpolar current, J. Phys. Oceanogr., 36, 1317–1331, 2006.

Vimont, D. J., Alexander, M., and Fontaine, A.: Midlatitude excitation of tropical variability in the pacific: The role of thermodynamic coupling and seasonality, J. Climate, 22, 518–534, doi:10.1175/2008JCLI2220.1, 2009.

Von Storch, H., Burger, G., Schnur, R. and Von Storch, J. S.: Principal oscillation patterns: a review, J. Climate, 8, 377–400, doi:10.1175/1520-0442(1995)008<0377:POPAR>2.0.CO;2, 1995.

Zebiak, S. E. and Cane, M. A.: A model El Niño-Southern Oscillation, Mon. Weather Rev., 115, 2262–2278, doi:10.1175/1520-0493(1987)115<2262:AMENO>2.0.CO;2, 1987.